THE JOURNAL OF PHYSICAL CHEMISTRY B
A JOURNAL OF THE AMERICAN CHEMICAL SOCIETY

pubs.acs.org/JPCB

Article

Structural and Dynamical Differences in the Spike Protein RBD in the SARS-CoV-2 Variants B.1.1.7 and B.1.351

Nisha Bhattarai, Prabin Baral, Bernard S. Gerstman, and Prem P. Chapagain*

Cite This: https://doi.org/10.1021/acs.jpcb.1c01626

Read Online

ACCESS | Metrics & More | Article Recommendations | Supporting Information

ABSTRACT: The novel coronavirus (SARS-CoV-2) pandemic that started in late 2019 is responsible for hundreds of millions of cases worldwide and millions of fatalities. Though vaccines are available, the virus is mutating to form new strains among which are the variants B.1.1.7 and B.1.351 that demonstrate increased transmissivity and infectivity. In this study, we performed molecular dynamics simulations to explore the role of the mutations in the interaction of the virus spike protein receptor binding domain (RBD) with the host receptor ACE2. We find that the hydrogen bond networks are rearranged in the variants and also that new hydrogen bonds are established between the RBD and ACE2 as a result of mutations. We investigated three variants: the wild-type (WT), B.1.1.7, and B.1.351. We find that the B.1.351 variant (also known as 501Y.V2) shows larger flexibility in the RBD loop segment involving residue K484, yet the RBD−ACE2 complex shows higher stability. Mutations that allow a more flexible interface that can result in a more stable complex may be a factor contributing to the increased infectivity of the mutated variants.

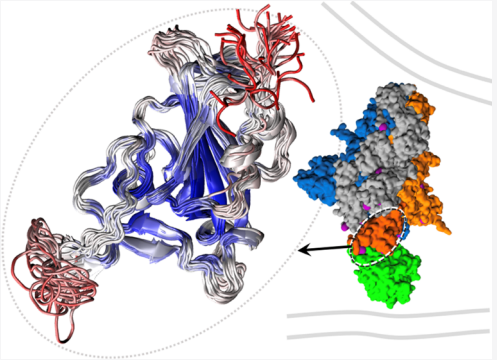

1. INTRODUCTION

The highly contagious severe acute respiratory syndrome coronavirus-2 (SARS-CoV-2) is a form of severe acute respiratory syndrome coronavirus (SARS) that had an outbreak in China in 2003 and causes the COVID-19 disease in a number of animal species including humans.[1−3] The first case of SARS-CoV-2 was detected in December 2019 in Wuhan, China, and a pandemic was declared in March 2020 due to its worldwide transmission. A person contracting this disease can have symptoms including fever, dry cough, headache, breathing difficulties, and pneumonia.[2−4] In January 2021, the number of SARS-CoV-2 cases surpassed 100 million worldwide with over 2 million deaths. Vaccines produced by Pfizer/BioNTech and Moderna have been authorized for emergency use in the United States after demonstrating efficacy in clinical trials.[5]

Despite the progress in vaccine administration, emergence of mutated variants is raising concerns about vaccine efficacies. Notably, the viruses that emerged in the United Kingdom (B.1.1.7 lineage) and separately in South Africa (B.1.351 lineage, also known as 501Y.V2) are reported to increase the transmission of the virus and host immune evasion.[6,7] In the spike protein alone, the B.1.1.7 variant has amino acid deletions at H69, V70, and Y144 and mutations N501Y, A570D, P681H, T716I, S982A, and D1118H, while the South African variant has mutations L18F, D80A, D215G, R246I, K417N, E484K, N501Y, and A701V.[8] The N501Y mutation at the receptor binding domain (RBD) that directly interacts with the human receptor ACE2, as shown in Figure 1, is found to be common in both of these mutants and is assumed to increase virus infectivity and transmittivity.[9] In the South African variant, mutations in the RBD (K417N, E484K, and N501Y) are thought to have functional significance.[10] The B.1.1.7 variant is reported to have a 71% higher transmission rate than the other variants.[11] The full significance of the B.1.351 variant is still unclear, and it is assumed that this lineage could be associated with increased transmissibility[10] and render current vaccines significantly less effective.[12]

The occurrence of mutated variants with increased rates of virus transmission and immune evasion has raised concern about the necessity of modifying existing vaccines and treatments.[12,13] Guidance for these interventions can benefit from an understanding of changes in the molecular mechanisms of infection as a result of the mutations, which is also essential for understanding the enhanced virulence of the mutated variants. Although some of the studies have been performed with these variants,[14] the details of amino acids that play crucial roles at the RBD−ACE2 interface yet remain unexplored. In this study, we investigated the changes in molecular bonding patterns between the spike protein-mutated RBD and the host ACE2 for the B.1.1.7 and B.1.351 variants compared to that of the wild-type (WT). We find that the mutations have significant effects by

Received: February 23, 2021
Revised: May 25, 2021

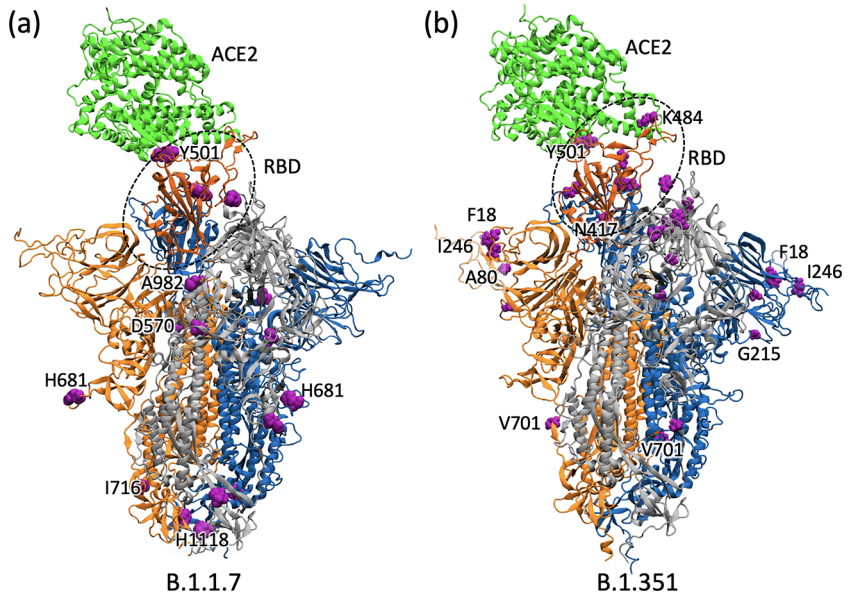

Figure 1. SARS-CoV-2 spike trimers with RBD-up structure complexed with ACE2 for (a) B.1.1.7 and (b) B.1.351 variants after relaxing with molecular dynamics (MD) simulation. The mutated residues are highlighted in purple.

changing the amino acids responsible for hydrogen bonding between the RBD and ACE2.

2. MATERIALS AND METHODS

2.1. System Preparation. A fully glycosylated SARS-CoV-2 spike trimer in which one of the receptor binding domains is facing upwards and complexed with ACE2 was retrieved from the archives of the CHARMM-GUI[15,16] COVID-19 repository (PDB ID 6VSB_6VW1).[17−19] This wild-type (WT) structure contains modeled glycan chains at the glycosylated sites and has the missing residues filled with GalaxyFill.[20,21] The mutations or deletions were then introduced to this WT structure using CHARMM-GUI.[16] We prepared a total of nine independent systems: the spike trimer complexed with ACE2, spike RBD−ACE2 complex, and RBD-only system for each of WT, B.1.1.7, and B.1.351 variants. Residues 1−1146 were considered in the spike trimer structure and 19−614 in the ACE2 domain. Similarly, the RBD residues 330−530 were used in the RBD-only as well as for the RBD−ACE2 complex systems, and residues 19−614 were used in the ACE2 domain. All nine systems were set up using the CHARMM-GUI Solution Builder tool with standard parameters, including a physiological salt concentration of 0.15 M KCl.

2.2. Molecular Dynamics Simulations. All-atom, explicit solvent molecular dynamics (MD) simulations were performed using the NAMD 2.13 simulation package[22] with the Charmm36m force field.[23,24] The covalent bonds involving hydrogen atoms were constrained by using the SHAKE algorithm,[25] and the pressure was controlled using the Nose−Hoover Langevin piston method[26] with a piston decay of 25 fs and a period of 50 fs. The particle mesh Ewald method[27] was used to calculate the long-range ionic interactions, and the temperature was controlled by using the Langevin temperature coupling with a friction coefficient of 1 ps^{-1}. Minimization and equilibration were performed with NVT (constant volume and temperature) conditions, and the production runs were performed under NPT (constant pressure and temperature) conditions at 303 K using 2 fs time steps. The RBD-only systems were run for 600 ns each, and the RBD−ACE2 systems were run for 200 ns each. Additional replicas of RBD-only systems were run for 300 ns. For all larger systems of spike protein trimer−ACE2 complexes (∼900 000 atoms), the production runs were limited to 50 ns each, which should be sufficient for the side-chain relaxations upon mutation but not for large-scale conformational changes. Visualization and rendering of trajectories were done with visual molecular dynamics (VMD).[28]

2.3. Dynamical Network Analysis. We used the Network Plugin in VMD[29,30] for dynamical network analysis calculations. Carma[31] and Catdcd[30] were used to calculate the covariance and correlations between interfacial amino acid pairs during an MD trajectory. To generate the amino acid community network, gncommunities[29] was employed. Using the Girvan−Newman algorithm, the time-averaged connectivity of the nodes was determined and the shortest path between the nodes for connections was also identified.[32]

2.4. Principal Component Analysis. The principal component analysis (PCA) of the Bio3D[33] software package was used to study the coordinated motions of amino acids and to understand the conformational motions of the atoms in all three systems. First, least-squares fitting is used to remove the translational and rotational motions of the proteins during the MD trajectory and the remaining motion of the protein atoms is analyzed.

3. RESULTS AND DISCUSSION

The spike protein of the B.1.1.7 variant has deletions of H69, V70, and Y144 and mutations N501Y, A570D, P681H, T716I, S982A, and D1118H amino acids. Similarly, the B.1.351 variant has mutations L18F, D80A, D215G, R246I, K417N, E484K, N501Y, and A701V. Figure 1 shows the mutations (highlighted in purple) in the spike trimer complexed with ACE2 in both B.1.1.7 and B.1.351 variants. The RBD of B.1.1.7 has only one mutation N501Y, whereas B.1.351 has N501Y and additional mutations K417N and E484K. To investigate the interactions with the human host receptor ACE2 in more detail, we focused on the RBD-only as well as the RBD−ACE2 complexes.

https://doi.org/10.1021/acs.jpcb.1c01626
J. Phys. Chem. B XXXX, XXX, XXX−XXX

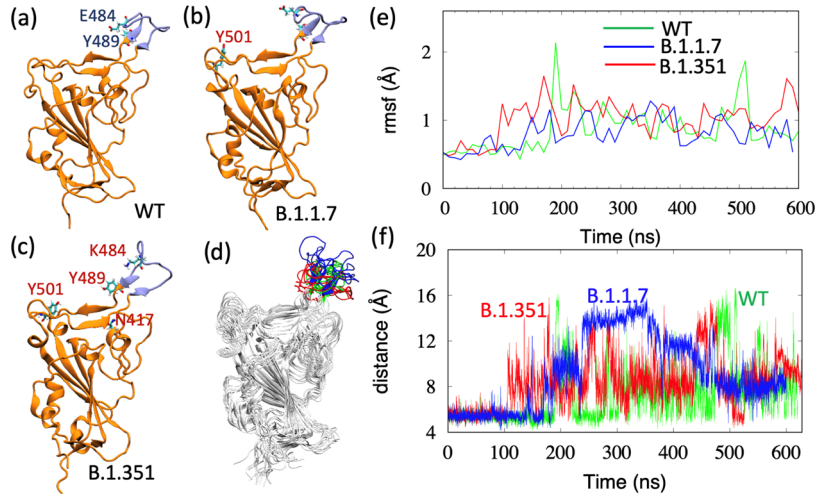

Figure 2. RBD structures at the end of 600 ns simulation for (a) WT, (b) B.1.1.7, and (c) B.1.351. The loop segments consisting of residues 473−489 are highlighted in blue. Mutations in the variants are labeled with red fonts. (d) Structural comparison of the five conformations of each variant, taken from the last 500 ns of the simulation (i.e., one frame every 100 ns). (e) Root-mean-square fluctuations (rmsf) as a function of time for residues 480−489 for all three variants: WT (green), B.1.1.7 (blue), and B.1.351 (red). (f) Distance between the C_α atoms of residues 484 and 489 showing large-scale motions of the loop segment. The rmsf and the distance graphs for the replica runs are plotted in Figure S3b,d.

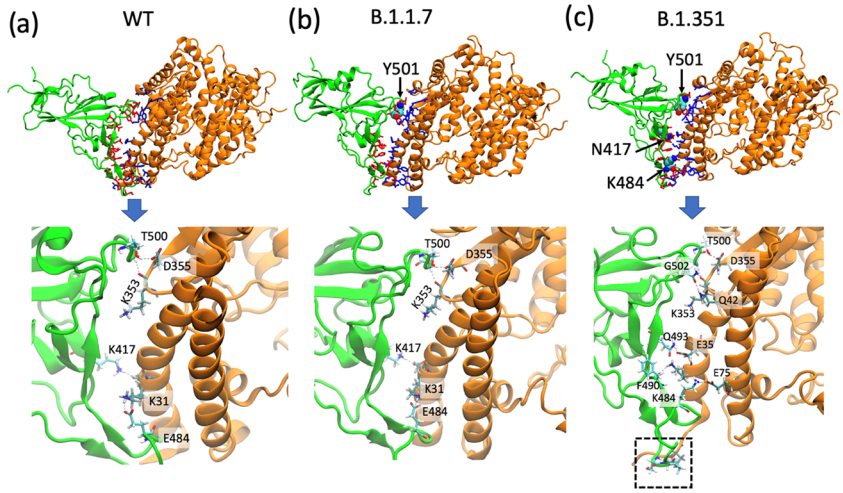

Figure 3. Snapshot of the RBD−ACE2 complex at 100 ns of MD simulation time: (a) WT, (b) B.1.1.7, and (c) B.1.351 variants. Top row: residues interacting within 3.5 Å of each other are highlighted in red for the RBD and blue for the ACE2 protein. The mutated residues in the B.1.1.7 and B.1.351 are labeled. Bottom row: residues forming interfacial hydrogen bonds between the viral spike RBD (green) and the host ACE2 (orange) WT, B.1.1.7, and B.1.351 variants. The highlighted box shows the residue pairs forming hydrogen bonds that only occur in the SA variant.

3.1. Structural Changes and Flexibility of the RBD Due to Mutations. Mutations in SARS-CoV-2 genes can lead to alterations in protein structures.[34] To investigate the changes in the RBD structure and dynamics due to mutations, we performed MD simulations of the RBD-only systems, not complexed with ACE2, for the three variants: WT, B.1.1.7 with the mutation N501Y, and B.1.351 with three mutations N501Y, K417N, and E484K. Figure 2a−c shows the RBD for the WT, B.1.1.7, and B.1.351 variants after 600 ns simulations. To visualize the structural flexibility of the RBD of each variant, we overlapped 20 conformations, taken one frame every 25 ns of the last 500 ns trajectory, as displayed in Figure S1. We colored each of these conformations according to the residues' root-mean-square fluctuations (rmsf), calculated for a 50 ns window that is centered at that specific frame. The overlapped structures, combined with the color gradients from blue−white−red, show that all variants have a flexible loop region (red) consisting of residues 473−489. Simulation of the B.1.351 variant shows significant structural changes in this loop region, which involves the mutation E484K, as shown in Figure 2c,d. This loop is an important RBD region as it is involved in binding with ACE2. To understand the conformational changes of the loop in B.1.351, we visualized the hydrogen-bonding pattern. For the B.1.351 variant, the initial hydrogen bonds break or weaken and the loop reorients (Figure S2a). In Figure S2b, we plotted the acceptor−donor distances between the important hydrogen-bond-forming residues for all three variants. The hydrogen bond Y473−Y489 remains intact for all three variants, whereas other hydrogen bonds fluctuate and differ. We superimposed five conformations of each variant from the last 500 ns (one conformation every 100 ns) and are displayed in Figure 2d, highlighting the flexible loop segment. To understand the flexibility of the loop region, we calculated the average root-mean-square fluctuations (rmsf) of the loop residues 480−489 for sliding windows of a width of 10 ns, with a total of 60 windows (Figure 2e). The average rmsf of the loop residues 480−489 shows that the residues in the

https://doi.org/10.1021/acs.jpcb.1c01626
J. Phys. Chem. B XXXX, XXX, XXX−XXX

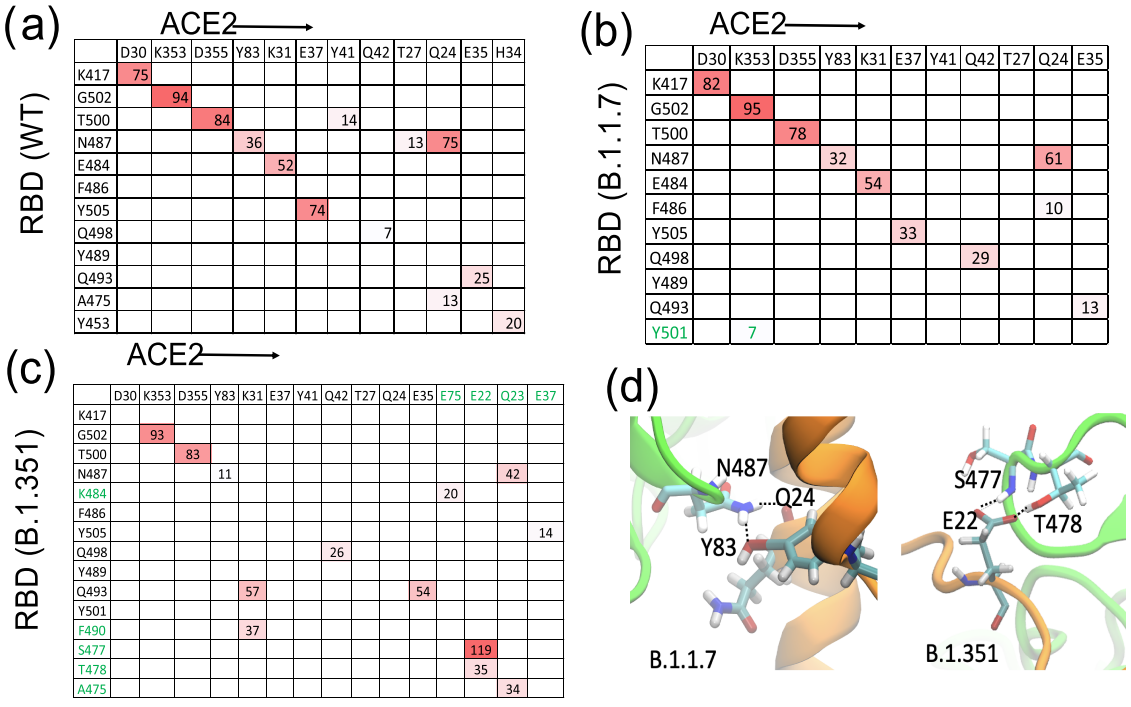

Figure 4. Interaction matrix for the residue pairs contributing to interprotein hydrogen bonding: (a) WT, (b) B.1.1.7, and (c) B.1.351 variants. The residue pairs are ordered in the matrices according to the percentage of hydrogen bond occupancy for the WT. The percentage of the hydrogen bonds that are unique to each variant is colored in green. (d) Prominent hydrogen bonds in each variant.

B.1.351 show larger fluctuations in general. While the loop in the WT shows occasional large motion, as shown by the distance between the C_α atoms of residues 484 and 489, this motion is different in the B.1.1.7 and B.1.351 variants (Figure 2f). The loop in the B.1.1.7 variant shows multiple semistable states. However, the loop is quite flexible in B.1.351 (Figures 2e,f and S2 and Movie S1). This observation is reproduced in the 300 ns replica run, which shows even clearer differences in the flexibility (Figure S3b,d). A flexible loop in B.1.351 may allow the RBD to bind with ACE2 more easily by induced fit mechanism. To investigate the binding with ACE2, we further explored the interactions in the RBD−ACE2 complexes.

3.2. RBD−ACE2 Interactions in the Variants. To understand the differences in the ACE2 binding, we explored the dynamics of the RBD−ACE2 complexes for all three variants. The analyses of the interaction pattern between the viral spike protein RBD and the receptor protein ACE2 from the 200 ns of MD simulations show that the B.1.1.7 and B.1.351 mutations have a significant impact on the association of residues in the interfacial region. Figure 3 shows the conformations of each system at 100 ns. The mutated residues are labeled, and the residues across the interface interacting within 3.5 Å of each other are highlighted.

To determine how the B.1.1.7 and B.1.351 variants differ from the WT in RBD−ACE2 bonding, we calculated the number of hydrogen bonds formed during the last 100 ns of the MD simulations. The residue pairs that have significant interaction between the RBD and the ACE2 are identified from the hydrogen bond occupancy rate for each residue pair. Some of the residues contributing to the formation of hydrogen bonds in the RBD−ACE2 complex for the WT, B.1.1.7, and B.1.351 variants are highlighted in Figure 3. Figure 4a−c shows the percentage of time that various interprotein hydrogen bonds existed during the last 100 ns of the simulations for the WT, B.1.1.7, and B.1.351 variants. The H-bonds of the RBD−ACE2 residue pairs G502−K353, T500−D355, Q498−Q42, and N487−Y83 occurred in all three complexes but with different occupancy probabilities. Some H-bonds in the WT become less important or disappear in the B.1.1.7 and B.1.351 variants but new hydrogen bonds S477−E22, T478−E22, and K484−E75 with high occupancy are observed in the B.1.351 variant. H-bonds unique to each system (i.e., present in one and absent in the remaining two) are displayed in Figure 4d.

Figure 4 shows that the strong salt-bridge interaction K417−D30 between RBD−ACE2 is present in both the WT and B.1.1.7 variants but not in the B.1.351 variant with the K417N mutation. In addition, another WT salt-bridge interaction E484−K31 is changed to K484−E75 in the B.1.351 variant. The S477−E22 and T478−E22 H-bond pairs in B.1.351 are especially interesting because they are absent in the WT and B.1.1.7 variants. Both of these H-bonds shown in Figure 4d are located at the terminal region of the interface (highlighted within the dotted box in Figure 3c). Overall, the hydrogen bond analysis shows one new H-bond (Y501−K353) in B.1.1.7 and eight new H-bonds (N487−Q23, K484−E75, Q493−K31, F490−K31, S477−E22, A475−Q23, Y505−E37, and T478−E22) in B.1.351. Despite the larger flexibility of the RBD interfacial region of the B.1.351 variant when not complexed with ACE2, the presence of the additional hydrogen bonds at the RBD−ACE2 interface suggests an enhanced specificity and the formation of a stable complex for this variant. We calculated the binding energies for the RBD−ACE2 complexes using PRODIGY webserver,[35] which utilizes the interfacial contacts and other properties such as polarity and charge at the interfaces to predict the binding affinity. The binding affinity values calculated for five different frames in the last 20 ns of the 200 ns run are shown in Table S2. These calculations show that the binding affinities are essentially the same in these variants, suggesting that the complexes have similar stabilities. To further

https://doi.org/10.1021/acs.jpcb.1c01626
J. Phys. Chem. B XXXX, XXX, XXX−XXX

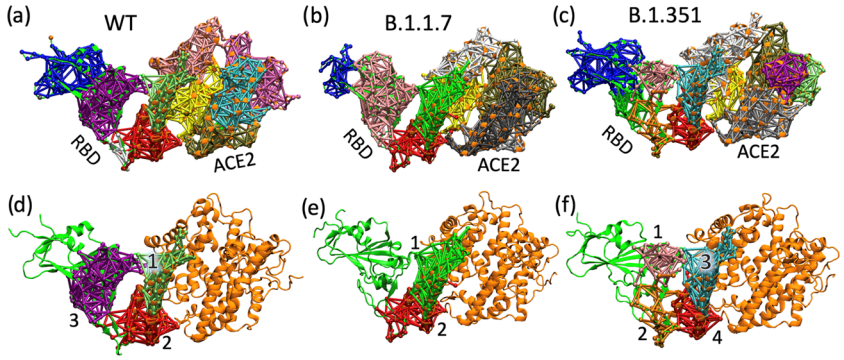

Figure 5. Dynamic network community analysis for (a) WT, (b) B.1.1.7, and (c) B.1.351 variants from the last 100 ns of the MD simulation trajectory. Communities that span the interface between the RBD and ACE2 are numbered 1−4 and shown in an expanded view for (d) WT (tan, red; 16 interprotein connections), (e) B.1.1.7 (silver, green, red; 18 interprotein connections), and (f) B.1351 (purple, gray, red; 18 interprotein connections).

explore the interprotein interactions and the stability of complexes, we performed dynamical network analysis.

3.3. Dynamic Correlated Motions in the Variants. The bonding interactions described above between the viral RBD and the host ACE2 are crucial in stabilizing the complex. The relative stability of the RBD−ACE2 complex for the different variants can be elucidated by investigating the conformational flexibility between the RBD and ACE2. We examined this by using a dynamical network analysis method. Dynamical network analysis quantifies connection networks and communities by examining correlated motions in proteins and nucleic acids.[29,36−38] It generates detailed information on the connections of amino acids in the form of communities and gives information about how strongly the amino acids are connected and how much their motion is correlated. Figure 5 shows various amino acid communities in the dynamic network obtained from the last 100 ns of the MD simulation. Amino acids are represented as nodes centered at the C_α, and the correlated motion between the amino acids is represented by the weighted edge (bar) between the nodes. The thickness of the edges represents the strength of the connections between the nodes. For nodes to be in the same community, they need to have a connection for more than 80% of the time.[29]

Figure 5a−c shows various dynamic network communities obtained for all variants, with each community colored differently. To visualize the interprotein interactions between the RBD and the ACE2, the communities that span over both of these proteins are highlighted in the expanded view of the interfacial region shown in Figure 5d−f. Amino acids present within the same community have highly correlated motions. This means that if a community spreads over the interface to include both the RBD and ACE2, the flexibility of the RBD with respect to the ACE2 is reduced. The amino acids in the RBD and ACE2 that compose each community and their interprotein connections are given in Table S1. The decrease in interfacial flexibility is notable for the B.1.351 variant, which has more and stronger interprotein connections (larger edge weights), compared to that in the WT and the B.1.1.7 variant. From these findings of the number of interprotein connections and the strength of the connections, it appears that the N501Y, E484K, and K417N mutations in the B.1.351 variant allow the formation of a stable RBD−ACE2 complex.

We further explored the conformational motions of these RBD−ACE2 complexes by using principal component analysis (PCA) with the 200 ns of the MD simulations. PCA is helpful in analyzing the motion of complicated systems with many particles and many internal degrees of freedom. The principal components describe the axes of maximal variance of the distribution of the structure. Eigenvectors represent coordinated motions in the fluctuations in atomic positions during the MD simulation, and the magnitude of the fluctuations of atoms is given by the corresponding eigenvalues. The first few eigenvectors represent the largest motion.

Figure S4 shows the range of motion from the principal components (PCs) 1 and 2 for each amino acid for the WT, B.1.17, and B.1.351 variants. The blurrier RBD in Figure S4a implies a greater range of motion for the WT, compared to that of the B.1.351 variant in Figure S4c. The conformational motion of the first three PCA eigenvectors PC1, PC2, and PC3 was projected onto 2D subspaces, as shown in Figure S4d−f. The conformational state of the system in each MD frame is represented by the blue and red dots. These distributions show that the WT complex has a greater conformational range than that of the mutated systems, with the B.1.351 showing more clustered PC1/PC2 and PC1/PC3. These findings are consistent with the results of the hydrogen bond and dynamical network analyses.

4. CONCLUSIONS

The SARS-CoV-2 spike protein is the major surface protein of the virion that is primarily responsible for the virus's ability to enter the human host through the ACE2 receptor. The interfacial region of the spike RBD−ACE2 complex plays a major role in the binding of the virus to the host cell. The emergence of mutated variants in the B.1.1.7 and B.1.351 raises concerns about alterations in the interprotein amino binding in this complex as well as in the efficacy of vaccines designed for the WT. Here, we have performed MD simulations and determined changes in the amino acids and their binding at the RBD−ACE2 interface due to the mutations in three different variants. We find that the RBD interfacial region shows a much larger flexibility in B.1.351 when not complexed with ACE2 but a stronger binding in the complex. The observed changes in the number and strength of the interprotein hydrogen bonds imply an enhanced specificity and binding in the B.1.351 variant, suggesting an optimized flexible interface that allows stronger binding via induced fit mechanism for this variant. Consistent with the stronger interprotein binding, dynamical network analysis and principal component analysis show that the RBD−ACE2 complex with the B.1.351 variant is less flexible. The question of how the flexibility of the RBD and the subtle changes in the interactions with ACE2 affect the virus's transmissibility or the

https://doi.org/10.1021/acs.jpcb.1c01626
J. Phys. Chem. B XXXX, XXX, XXX−XXX

vaccine efficacy for a variant is difficult to address but these studies provide information on the molecular interactions of RBD−ACE2 complexes in different variants, and it can be important for understanding the molecular mechanism of the virus entry into the cell and designing therapeutic interventions. Further studies are needed to understand the full scope of the effects resulting from the mutations or deletions. For example, the mutations may affect trimer formation or trimer stability. In fact, it is recently shown that the D614G mutation enhances the spike protein trimer stability and prevents premature release of S1 subunit.[39] It will be useful to know how the mutations affect the springing up of the RBD from the closed conformation that is shielded with glycans[40,41] or how the mutations in the rest of the spike, including the ones in the furin cleavage site,[42,43] affect the mechanism of virus entry, infectivity, or immune evasion.

■ ASSOCIATED CONTENT

Supporting Information

The Supporting Information is available free of charge at https://pubs.acs.org/doi/10.1021/acs.jpcb.1c01626.

Additional figures showing the flexibility and hydrogen bonding, tables showing RBD−ACE2 connectivity and binding affinity, and Movie S1 showing the 600 ns trajectories for the variants (PDF)

Movie S1: MD trajectories for the WT, B.1.1.7, and B.1.351 variants (MOV)

■ AUTHOR INFORMATION

Corresponding Author

Prem P. Chapagain − *Department of Physics, Florida International University, Miami, Florida 33199, United States; Biomolecular Sciences Institute, Florida International University, Miami, Florida 33199, United States;* orcid.org/0000-0002-0999-4975; Email: chapagap@fiu.edu

Authors

Nisha Bhattarai − *Department of Physics, Florida International University, Miami, Florida 33199, United States;* orcid.org/0000-0002-5595-1474

Prabin Baral − *Department of Physics, Florida International University, Miami, Florida 33199, United States*

Bernard S. Gerstman − *Department of Physics, Florida International University, Miami, Florida 33199, United States; Biomolecular Sciences Institute, Florida International University, Miami, Florida 33199, United States;* orcid.org/0000-0003-4258-529X

Complete contact information is available at: https://pubs.acs.org/10.1021/acs.jpcb.1c01626

Notes

The authors declare no competing financial interest.

■ ACKNOWLEDGMENTS

This work was partially supported by the National Science Foundation under Grant No. 2037374. NB acknowledges the Dissertation Year Fellowship support from the University Graduate School at Florida International University. The authors thank Prof. Giri Narasimhan at Florida International University for helpful discussions.

■ REFERENCES

(1) Rota, P. A.; Oberste, M. S.; Monroe, S. S.; Nix, W. A.; Campagnoli, R.; Icenogle, J. P.; Penaranda, S.; Bankamp, B.; Maher, K.; Chen, M. H.; Tong, S.; Tamin, A.; Lowe, L.; Frace, M.; DeRisi, J. L.; Chen, Q.; Wang, D.; Erdman, D. D.; Peret, T. C.; Burns, C.; Ksiazek, T. G.; Rollin, P. E.; Sanchez, A.; Liffick, S.; Holloway, B.; Limor, J.; McCaustland, K.; Olsen-Rasmussen, M.; Fouchier, R.; Gunther, S.; Osterhaus, A. D.; Drosten, C.; Pallansch, M. A.; Anderson, L. J.; Bellini, W. J. Characterization of a novel coronavirus associated with severe acute respiratory syndrome. *Science* **2003**, *300*, 1394−1399.

(2) Wu, F.; Zhao, S.; Yu, B.; Chen, Y. M.; Wang, W.; Song, Z. G.; Hu, Y.; Tao, Z. W.; Tian, J. H.; Pei, Y. Y.; Yuan, M. L.; Zhang, Y. L.; Dai, F. H.; Liu, Y.; Wang, Q. M.; Zheng, J. J.; Xu, L.; Holmes, E. C.; Zhang, Y. Z. A new coronavirus associated with human respiratory disease in China. *Nature* **2020**, *579*, 265−269.

(3) Zhou, P.; Yang, X. L.; Wang, X. G.; Hu, B.; Zhang, L.; Zhang, W.; Si, H. R.; Zhu, Y.; Li, B.; Huang, C. L.; Chen, H. D.; Chen, J.; Luo, Y.; Guo, H.; Jiang, R. D.; Liu, M. Q.; Chen, Y.; Shen, X. R.; Wang, X.; Zheng, X. S.; Zhao, K.; Chen, Q. J.; Deng, F.; Liu, L. L.; Yan, B.; Zhan, F. X.; Wang, Y. Y.; Xiao, G. F.; Shi, Z. L. A pneumonia outbreak associated with a new coronavirus of probable bat origin. *Nature* **2020**, *579*, 270−273.

(4) Cui, J.; Li, F.; Shi, Z. L. Origin and evolution of pathogenic coronaviruses. *Nat. Rev. Microbiol.* **2019**, *17*, 181−192.

(5) Krammer, F. SARS-CoV-2 vaccines in development. *Nature* **2020**, *586*, 516−527.

(6) Kemp, S.; Harvey, W.; Datir, R.; Collier, D.; Ferreira, I.; Carabelli, A.; Robertson, D.; Gupta, R. Recurrent emergence and transmission of a SARS-CoV-2 Spike deletion ΔH69/V70 *bioRxiv* 2020, DOI: 10.1101/2020.12.14.422555.

(7) Andreano, E.; Piccini, G.; Licastro, D.; Casalino, L.; Johnson, N. V.; Paciello, I.; Monego, S. D.; Pantano, E.; Manganaro, N.; Manenti, A.; Manna, R.; Casa, E.; Hyseni, I.; Benincasa, L.; Montomoli, E.; Amaro, R. E.; McLellan, J. S.; Rappuoli, R. SARS-CoV-2 escape in vitro from a highly neutralizing COVID-19 convalescent plasma *bioRxiv* 2020, DOI: 10.1101/2020.12.28.424451.

(8) Naveca, F.; Nascimento, V.; Souza, V.; Corado, A.; Nascimento, F.; Silva, G.; Costa, Á.; Duarte, D.; Pessoa, K.; Gonçalves, L. Phylogenetic relationship of SARS-CoV-2 sequences from Amazonas with emerging Brazilian variants harboring mutations E484K and N501Y in the Spike protein.

(9) Wise, J. Covid-19: New coronavirus variant is identified in UK. *BMJ* **2020**, *371*, No. m4857.

(10) Tegally, H.; Wilkinson, E.; Giovanetti, M.; Iranzadeh, A.; Fonseca, V.; Giandhari, J.; Doolabh, D.; Pillay, S.; San, E. J.; Msomi, N. Emergence and rapid spread of a new severe acute respiratory syndrome-related coronavirus 2 (SARS-CoV-2) lineage with multiple spike mutations in South Africa *medRxiv* 2020, DOI: 10.1101/2020.12.21.20248640.

(11) Mahase, E. Covid-19: What have we learnt about the new variant in the UK? *BMJ* **2020**, *371*, No. m4944.

(12) Callaway, E.; Ledford, H. How to redesign COVID vaccines so they protect against variants. *Nature* **2021**, *590*, 15−16.

(13) Wang, Z.; Schmidt, F.; Weisblum, Y.; Muecksch, F.; Barnes, C. O.; Finkin, S.; Schaefer-Babajew, D.; Cipolla, M.; Gaebler, C.; Lieberman, J. A.; Yang, Z.; Abernathy, M. E.; Huey-Tubman, K. E.; Hurley, A.; Turroja, M.; West, K. A.; Gordon, K.; Millard, K. G.; Ramos, V.; Da Silva, J.; Xu, J.; Colbert, R. A.; Patel, R.; Dizon, J.; Unson-O'Brien, C.; Shimeliovich, I.; Gazumyan, A.; Caskey, M.; Bjorkman, P. J.; Casellas, R.; Hatziioannou, T.; Bieniasz, P. D.; Nussenzweig, M. C. mRNA vaccine-elicited antibodies to SARS-CoV-2 and circulating variants *bioRxiv* 2021, DOI: 10.1101/2021.01.15.426911.

(14) Nelson, G.; Buzko, O.; Spilman, P. R.; Niazi, K.; Rabizadeh, S.; Soon-Shiong, P. R. Molecular dynamic simulation reveals E484K mutation enhances spike RBD-ACE2 affinity and the combination of E484K, K417N and N501Y mutations (501Y. V2 variant) induces conformational change greater than N501Y mutant alone, potentially resulting in an escape mutant *bioRxiv* 2021, DOI: 10.1101/2021.01.13.426558.

(15) Woo, H.; Park, S. J.; Choi, Y. K.; Park, T.; Tanveer, M.; Cao, Y.; Kern, N. R.; Lee, J.; Yeom, M. S.; Croll, T. I.; Seok, C.; Im, W. Developing a Fully Glycosylated Full-Length SARS-CoV-2 Spike Protein Model in a Viral Membrane. *J. Phys. Chem. B* **2020**, *124*, 7128−7137.
(16) Jo, S.; Kim, T.; Iyer, V. G.; Im, W. CHARMM-GUI: a web-based graphical user interface for CHARMM. *J. Comput. Chem.* **2008**, *29*, 1859−1865.
(17) Shang, J.; Ye, G.; Shi, K.; Wan, Y.; Luo, C.; Aihara, H.; Geng, Q.; Auerbach, A.; Li, F. Structural basis of receptor recognition by SARS-CoV-2. *Nature* **2020**, *581*, 221−224.
(18) Berman, H. M.; Westbrook, J.; Feng, Z.; Gilliland, G.; Bhat, T. N.; Weissig, H.; Shindyalov, I. N.; Bourne, P. E. The protein data bank. *Nucleic Acids Res.* **2000**, *28*, 235−242.
(19) Wrapp, D.; Wang, N.; Corbett, K. S.; Goldsmith, J. A.; Hsieh, C. L.; Abiona, O.; Graham, B. S.; McLellan, J. S. Cryo-EM structure of the 2019-nCoV spike in the prefusion conformation. *Science* **2020**, *367*, 1260−1263.
(20) Ko, J.; Lee, D.; Park, H.; Coutsias, E. A.; Lee, J.; Seok, C. The FALC-Loop web server for protein loop modeling. *Nucleic Acids Res.* **2011**, *39*, W210−W214.
(21) Ko, J.; Park, H.; Seok, C. GalaxyTBM: template-based modeling by building a reliable core and refining unreliable local regions. *BMC Bioinf.* **2012**, *13*, No. 198.
(22) Phillips, J. C.; Braun, R.; Wang, W.; Gumbart, J.; Tajkhorshid, E.; Villa, E.; Chipot, C.; Skeel, R. D.; Kale, L.; Schulten, K. Scalable molecular dynamics with NAMD. *J. Comput. Chem.* **2005**, *26*, 1781−1802.
(23) Huang, J.; MacKerell, A. D., Jr. CHARMM36 all-atom additive protein force field: validation based on comparison to NMR data. *J. Comput. Chem.* **2013**, *34*, 2135−2145.
(24) Huang, J.; MacKerell, A. D., Jr. Force field development and simulations of intrinsically disordered proteins. *Curr. Opin. Struct. Biol.* **2018**, *48*, 40−48.
(25) Ryckaert, J.-P.; Ciccotti, G.; Berendsen, H. J. Numerical integration of the cartesian equations of motion of a system with constraints: molecular dynamics of n-alkanes. *J. Comput. Phys.* **1977**, *23*, 327−341.
(26) Brooks, M. M.; Hallstrom, A.; Peckova, M. A simulation study used to design the sequential monitoring plan for a clinical trial. *Stat. Med.* **1995**, *14*, 2227−2237.
(27) Essmann, U.; Perera, L.; Berkowitz, M. L.; Darden, T.; Lee, H.; Pedersen, L. G. A smooth particle mesh Ewald method. *J. Chem. Phys* **1995**, *103*, 8577−8593.
(28) Humphrey, W.; Dalke, A.; Schulten, K. VMD: visual molecular dynamics. *J. Mol. Graphics* **1996**, *14*, 33−38. 27-8.
(29) Sethi, A.; Eargle, J.; Black, A. A.; Luthey-Schulten, Z. Dynamical networks in tRNA:protein complexes. *Proc. Natl. Acad. Sci. U.S.A.* **2009**, *106*, 6620−6625.
(30) Eargle, J.; Luthey-Schulten, Z. NetworkView: 3D display and analysis of protein.RNA interaction networks. *Bioinformatics* **2012**, *28*, 3000−3001.
(31) Glykos, N. M. Software news and updates. Carma: a molecular dynamics analysis program. *J. Comput. Chem.* **2006**, *27*, 1765−1768.
(32) Girvan, M.; Newman, M. E. Community structure in social and biological networks. *Proc. Natl. Acad. Sci. U.S.A.* **2002**, *99*, 7821−7826.
(33) Grant, B. J.; Rodrigues, A. P.; ElSawy, K. M.; McCammon, J. A.; Caves, L. S. Bio3d: an R package for the comparative analysis of protein structures. *Bioinformatics* **2006**, *22*, 2695−2696.
(34) Wu, S.; Tian, C.; Liu, P.; Guo, D.; Zheng, W.; Huang, X.; Zhang, Y.; Liu, L. Effects of SARS-CoV-2 mutations on protein structures and intraviral protein-protein interactions. *J. Med. Virol.* **2021**, *93*, 2132−2140.
(35) Xue, L. C.; Rodrigues, J. P.; Kastritis, P. L.; Bonvin, A. M.; Vangone, A. PRODIGY: a web server for predicting the binding affinity of protein-protein complexes. *Bioinformatics* **2016**, *32*, 3676−3678.
(36) Gc, J. B.; Gerstman, B. S.; Chapagain, P. P. The Role of the Interdomain Interactions on RfaH Dynamics and Conformational Transformation. *J. Phys. Chem. B* **2015**, *119*, 12750−12759.
(37) McClendon, C. L.; Kornev, A. P.; Gilson, M. K.; Taylor, S. S. Dynamic architecture of a protein kinase. *Proc Natl. Acad. Sci. U.S.A.* **2014**, *111*, E4623−E4631.
(38) Alexander, R. W.; Eargle, J.; Luthey-Schulten, Z. Experimental and computational determination of tRNA dynamics. *FEBS Lett.* **2010**, *584*, 376−386.
(39) Zhang, J.; Cai, Y.; Xiao, T.; Lu, J.; Peng, H.; Sterling, S. M.; Walsh, R. M., Jr.; Rits-Volloch, S.; Zhu, H.; Woosley, A. N.; Yang, W.; Sliz, P.; Chen, B. Structural impact on SARS-CoV-2 spike protein by D614G substitution. *Science* **2021**, *372*, 525−530.
(40) Henderson, R.; Edwards, R. J.; Mansouri, K.; Janowska, K.; Stalls, V.; Gobeil, S. M. C.; Kopp, M.; Li, D.; Parks, R.; Hsu, A. L.; Borgnia, M. J.; Haynes, B. F.; Acharya, P. Controlling the SARS-CoV-2 spike glycoprotein conformation. *Nat. Struct. Mol. Biol.* **2020**, *27*, 925−933.
(41) Berger, I.; Schaffitzel, C. The SARS-CoV-2 spike protein: balancing stability and infectivity. *Cell Res.* **2020**, *30*, 1059−1060.
(42) Xia, S.; Lan, Q.; Su, S.; Wang, X.; Xu, W.; Liu, Z.; Zhu, Y.; Wang, Q.; Lu, L.; Jiang, S. The role of furin cleavage site in SARS-CoV-2 spike protein-mediated membrane fusion in the presence or absence of trypsin. *Signal Transduction Targeted Ther.* **2020**, *5*, No. 92.
(43) Papa, G.; Mallery, D. L.; Albecka, A.; Welch, L. G.; Cattin-Ortola, J.; Luptak, J.; Paul, D.; McMahon, H. T.; Goodfellow, I. G.; Carter, A.; Munro, S.; James, L. C. Furin cleavage of SARS-CoV-2 Spike promotes but is not essential for infection and cell-cell fusion. *PLoS Pathog.* **2021**, *17*, No. e1009246.

https://doi.org/10.1021/acs.jpcb.1c01626
J. Phys. Chem. B XXXX, XXX, XXX−XXX